

A new fast multipole boundary element method for solving large-scale two-dimensional elastostatic problems

Yijun Liu*,†

Department of Mechanical, Industrial and Nuclear Engineering, University of Cincinnati, P.O. Box 210072, Cincinnati, OH 45221-0072, U.S.A.

SUMMARY

A new fast multipole boundary element method (BEM) is presented in this paper for large-scale analysis of two-dimensional (2-D) elastostatic problems based on the direct boundary integral equation (BIE) formulation. In this new formulation, the fundamental solution for 2-D elasticity is written in a complex form using the two complex potential functions in 2-D elasticity. In this way, the multipole and local expansions for 2-D elasticity BIE are directly linked to those for 2-D potential problems. Furthermore, their translations (moment to moment, moment to local, and local to local) turn out to be exactly the same as those in the 2-D potential case. This formulation is thus very compact and more efficient than other fast multipole approaches for 2-D elastostatic problems using Taylor series expansions of the fundamental solution in its original form. Several numerical examples are presented to study the accuracy and efficiency of the developed fast multipole BEM formulation and code. BEM models with more than one million equations have been solved successfully on a laptop computer. These results clearly demonstrate the potential of the developed fast multipole BEM for solving large-scale 2-D elastostatic problems. Copyright © 2005 John Wiley & Sons, Ltd.

KEY WORDS: fast multipole method; boundary element method; 2-D elastostatic problems

1. INTRODUCTION

The boundary integral equation (BIE) formulations and their numerical solutions using boundary element method (BEM) for two-dimensional (2-D) elasticity problems were developed by Rizzo about 40 years ago [1]. Following this early work, extensive research efforts have been made for the development of the BIE/BEM for solving various elasticity problems (see, e.g. References [2–6]). However, the BEM has been limited to solving elasticity problems with a few thousands equations in most cases for many years, in spite of its ease in the modelling stage. This is because the conventional BEM in general produces dense and non-symmetrical matrices that, although smaller in sizes, require $O(N^2)$ operations to compute the coefficients

*Correspondence to: Yijun Liu, Department of Mechanical, Industrial and Nuclear Engineering, University of Cincinnati, P.O. Box 210072, Cincinnati, OH 45221-0072, U.S.A.

†E-mail: Yijun.Liu@uc.edu

Received 30 April 2005

Revised 22 July 2005

Accepted 22 July 2005

and another $O(N^3)$ operations to solve the system using direct solvers (where N is the number of equations).

In the mid-1980s, Rokhlin and Greengard [7–9] pioneered the innovative fast multipole method (FMM) that can be used to accelerate the solutions of boundary integral equations, promising to reduce the CPU time and memory requirement in the fast multipole accelerated BEM to $O(N)$. The introduction of the FMM in the BEM has generated enormous interests in the BEM, that is now not only easy in meshing of complicated geometries, accurate for solving singular fields or fields in infinite domains, but also practical and often superior in solving large-scale problems. Some of the early research on fast multipole BEM for elasticity problems can be found in References [10–21], which show great promises of the BEM for solving large-scale elasticity related problems. Most recently, 3-D composite material models containing tens of thousands of fibres [22, 23] have been solved successfully by using the fast multipole BEM within hours and with moderate computing resources. A comprehensive review of the fast multipole BIE/BEM can be found in Reference [24].

Formulations in the fast multipole BEM for elasticity problems have not been convergent. Many approaches have been proposed regarding how to expand the kernel functions (fundamental solutions) and how to translate the coefficients of these expansions. The original FMM proposed by Rokhlin and Greengard [7–9] for 2-D potential problems is based on using functions with complex variables and expanding these complex functions using Taylor series expansions. However, extending Taylor series expansion approach for the kernel functions literally to 3-D problems have been found to be inefficient that requires large numbers of terms in the expansions and many iterations for convergence of the solutions. This difficulty lies in the fact that for 2-D problems using complex variables, each term in the Taylor series expansion is an analytic function with both real and imaginary parts being *harmonic* functions. Since the fundamental solution is also a harmonic function in nature, the Taylor series expansion in complex variables for 2-D is a natural choice, as it was used in the earlier works by Rokhlin and Greengard [7–9]. However, this is not the case for 3-D Taylor series expansion with *real* variables. Each term in such Taylor series expansions for 3-D problems does not resemble closely the behaviours of the 3-D kernel functions. A better choice for 3-D problems should be to employ *solid harmonic* or other harmonic functions in the expansions of the kernel functions (see, e.g. References [14, 15, 25, 26]), which can be considered as a 3-D counter-part of the 2-D case using complex variables. Expansions using solid harmonic functions with about 10–15 terms and about 20 iterations are often found to be sufficient for the convergence with a tolerance of 10^{-6} in the solutions of large 3-D problems with more than 10 million BEM equations [22, 23].

For 2-D elasticity problems using fast multipole BEM, there are several approaches as well. Greengard *et al.* [11, 12] used a fast multipole formulation for directly solving the biharmonic equations in 2-D elasticity. They applied Sherman's complex variable formulation to solve the biharmonic equation and presented several interesting large-scale problems. Peirce and Napier [10] developed a spectral multipole approach, that shares some common features with the FMMs. In their approach, a set of background grids are generated and Taylor series expansions of the kernels are used to compute the integrals at the grid points. Interpolations of these values give the values at the collocation points. This approach is of order $O(N \log N)$ in computational complexity. Richardson *et al.* [16] proposed a similar spectral method using both 2-D conventional and traction BIEs in the regularized form. Most recently, Yao *et al.* [21] studied 2-D multi-domain elasticity problems for modelling composite materials. They expanded the kernel functions in their original forms using complex Taylor series in an auxiliary way,

following Reference [27]. However, these expansions of the kernels are lengthy and the number of terms needed in the expansions is large and convergence is slow, as shown in the example problems in Reference [21].

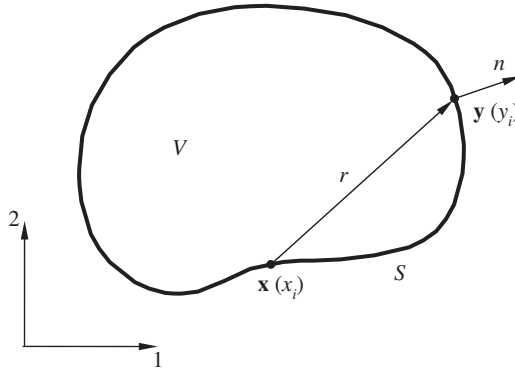
The elasticity problem and its direct BIE formulations are closely related to the potential problem and its direct BIE formulation. There should be a direct link between the fast multipole BEM for elasticity and that for potential problems in the same dimension. Expanding the key term $1/r$ in the kernels (with r being the distance between the collocation and integration points) using solid harmonic functions seems to be the link between 3-D elasticity and potential problems [14, 15, 25, 26]. For 2-D elasticity and potential problems, this link should be to expand the $\log(r)$ term in the kernels using functions of complex variables. This is evident because for 2-D elasticity problems, the solution due to a point force can be readily represented by two analytic functions of complex variables with the \log term [28, 29], which can be used directly to represent the kernels in the direct BIE formulation. The BIEs for 2-D elasticity, especially those for crack problems, have also been written in various forms with complex variables (see, e.g. References [30–38]). Fukui [32] seems to be the first to use the BIE in the complex form to develop the fast multipole BEM for 2-D elasticity problems. He expanded the two analytic functions directly in representing the integrals of the two kernels and defined two moments for each kernel. However, the moment-to-moment (M2M), moment-to-local (M2L) and local-to-local (L2L) expansions in his approach are different for the two moments and also different from those in the corresponding 2-D potential problems. Thus, this formulation is not compact and the relation to the 2-D potential fast multipole BEM is not evident.

In this paper, a new fast multipole BEM formulation is presented for 2-D elasticity problems based on the direct BIE formulation. The displacement and traction kernels are represented using the two complex analytic functions in 2-D elasticity [28, 29]. However, instead of expanding the two analytic functions directly, terms in the kernel functions, together with the density functions, are first re-grouped and then expanded to form two moments for each kernel. In this way, the multipole and local expansions for 2-D elasticity BIE are very similar to those for 2-D potential problems. Furthermore, their translations (M2M, M2L, and L2L) are symmetrical about the two moments and also identical to those in the 2-D potential case. This formulation is thus very compact and easy to program based on the corresponding 2-D potential code. It is also much more efficient than other fast multipole approaches using Taylor series expansions of the kernels with real variables. Several numerical examples are presented to study the accuracy and efficiency of the developed fast multipole BEM formulation and code. BEM models with more than one million equations have been solved successfully on a mid-range laptop computer. The required number of terms in the expansions is between 15 and 20 and the solutions can converge between 3 and 30 iterations for a tolerance of 10^{-6} . These results clearly demonstrate the potential of the developed fast multipole BEM for solving large-scale 2-D elastostatic problems.

2. THE NEW FAST MULTIPOLE BEM FORMULATION

We start with the following direct boundary integral equation for general 2-D elastostatic problems [1–6]:

$$C_{ij}(\mathbf{x})u_j(\mathbf{x}) = \int_S [U_{ij}(\mathbf{x}, \mathbf{y})t_j(\mathbf{y}) - T_{ij}(\mathbf{x}, \mathbf{y})u_j(\mathbf{y})] dS(\mathbf{y}) \quad \forall \mathbf{x} \in S \quad (1)$$

Figure 1. Domain V and boundary S .

where u_i and t_i are the displacement and traction, respectively; S the boundary of domain V (Figure 1); $C_{ij}(\mathbf{x})$ coefficients that are equal to $\frac{1}{2}\delta_{ij}$ if S is smooth around \mathbf{x} (δ_{ij} is the Kronecker δ); and $i, j = 1, 2$ in 2-D cases. The two kernel functions $U_{ij}(\mathbf{x}, \mathbf{y})$ and $T_{ij}(\mathbf{x}, \mathbf{y})$ in Equation (1) are the displacement and traction components in the fundamental solution (also called Kelvin's solution) given by the following expressions [1–6]:

$$U_{ij}(\mathbf{x}, \mathbf{y}) = \frac{1}{8\pi\mu(1-v)} \left[(3-4v)\delta_{ij} \log\left(\frac{1}{r}\right) + r_{,i} r_{,j} - \frac{1}{2} \delta_{ij} \right] \quad (2)$$

$$T_{ij}(\mathbf{x}, \mathbf{y}) = -\frac{1}{4\pi(1-v)r} \left\{ \frac{\partial r}{\partial n} [(1-2v)\delta_{ij} + 2r_{,i} r_{,j}] - (1-2v)(r_{,i} n_j - r_{,j} n_i) \right\} \quad (3)$$

for the plane strain case, in which μ is the shear modulus, v Poisson's ratio, $r = r(\mathbf{x}, \mathbf{y})$ the distance between the collocation point \mathbf{x} and integration point \mathbf{y} , n the outward normal (Figure 1), and $(\cdot)_{,i} = \partial(\cdot)/\partial y_i$. For the plane stress case, v is replaced by $v/(1+v)$ in expressions (2) and (3). The constant term $-\frac{1}{2}\delta_{ij}$ in expression (2), which does not affect the BIE solution, is added for the convenience in the multipole expansions of the kernels to be described in the following.

In the fast multipole BEM, for which iterative solvers such as GMRES are employed, fast summation methods are devised to evaluate the matrix–vector multiplications in the linear system $\mathbf{A}\lambda = \mathbf{b}$. These matrix–vector multiplications come from the two integrals in BIE (1) with estimated density functions (u_i or t_i) in the iterative solution process. Direct integrations as in the conventional BEM approach are used, when the collocation point \mathbf{x} is close to the boundary of integration. However, when \mathbf{x} is far away from the boundary of integration, the FMM is employed to evaluate the two integrals in Equation (1). To describe the new fast multipole formulation for 2-D elastostatic problems, we rewrite the two integrals in Equation (1) in the following form:

$$\begin{Bmatrix} \Delta_1(\mathbf{x}) \\ \Delta_2(\mathbf{x}) \end{Bmatrix}_t = \int_{S_0} \begin{bmatrix} U_{11}(\mathbf{x}, \mathbf{y}) & U_{12}(\mathbf{x}, \mathbf{y}) \\ U_{21}(\mathbf{x}, \mathbf{y}) & U_{22}(\mathbf{x}, \mathbf{y}) \end{bmatrix} \begin{Bmatrix} t_1(\mathbf{y}) \\ t_2(\mathbf{y}) \end{Bmatrix} dS(\mathbf{y}) \quad (4)$$

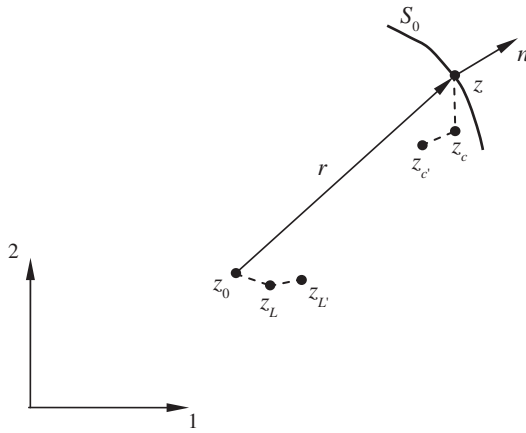


Figure 2. Complex notation and the related points for fast multipole expansions.

$$\begin{Bmatrix} \Delta_1(\mathbf{x}) \\ \Delta_2(\mathbf{x}) \end{Bmatrix}_u = \int_{S_0} \begin{bmatrix} T_{11}(\mathbf{x}, \mathbf{y}) & T_{12}(\mathbf{x}, \mathbf{y}) \\ T_{21}(\mathbf{x}, \mathbf{y}) & T_{22}(\mathbf{x}, \mathbf{y}) \end{bmatrix} \begin{Bmatrix} u_1(\mathbf{y}) \\ u_2(\mathbf{y}) \end{Bmatrix} dS(\mathbf{y}) \quad (5)$$

where S_0 is a subset of S and far away from the collocation point \mathbf{x} (Figure 2).

In 2-D elasticity theory using complex variables, the displacement field U_i at a point $z (= y_1 + iy_2$, with $i = \sqrt{-1}$) due to a point force $P = P_1 + iP_2$ at $z=0$ can be written as [28, 29]

$$U_1(z) + iU_2(z) = \frac{1}{2\mu} [\kappa\varphi(z) - z\overline{\varphi'(z)} - \overline{\chi'(z)}] \quad (6)$$

where the two complex analytic functions can be chosen as

$$\varphi(z) = -\frac{P}{2\pi(1+\kappa)} \log(z), \quad \chi(z) = \frac{\kappa\bar{P}}{2\pi(1+\kappa)} [z \log(z) - z] \quad (7)$$

in which $(\bar{})$ indicates the complex conjugate, and $\kappa = 3 - 4\nu$ for the plane strain case. Substituting (7) into (6), we can write

$$U_1(z) + iU_2(z) = \frac{1}{4\pi\mu(1+\kappa)} \left[-\kappa P \log(z) + \bar{P} \frac{z}{\bar{z}} - \kappa P \overline{\log(z)} \right] \quad (8)$$

From Equation (8), we can obtain the fundamental solution U_{ij} exactly as given in Equation (2). It can also be shown that the integral in (4) can be written in the following form by applying Equation (8) (with $z_0 = x_1 + ix_2$):

$$\begin{aligned} D_t(z_0) &\equiv [\Delta_1(\mathbf{x}) + i\Delta_2(\mathbf{x})]_t \\ &= \frac{1}{4\pi\mu(1+\kappa)} \int_{S_0} \left[-\kappa \log(z_0 - z) t(z) + \frac{(z_0 - z)}{(z_0 - z)} \overline{t(z)} - \kappa \overline{\log(z_0 - z)} t(z) \right] dS(z) \end{aligned} \quad (9)$$

where $t = t_1 + it_2$ is the traction. This integral can be used to evaluate readily the contributions from the U kernel integral in BIE (1). In Reference [32], Fukui expanded separately the two analytic functions as given in Equation (7) (with a slightly different form for χ) to define two moments and used Equation (6) to evaluate the total contribution in the fast multipole approach. This results in various different expressions of the translations for the moments and local expansions that also differ from those in the 2-D potential case.

In fact, it is more convenient to expand the functions in Equation (9) in groups with respect to the Green's function for 2-D potential problems. In this way, the translations and local expansions turn out to be symmetrical for the two moments and identical to those used in the 2-D potential problems. To proceed, we rewrite Equation (9) in the following form:

$$D_t(z_0) = \frac{1}{4\pi\mu(1+\kappa)} \int_{S_0} [\kappa G(z_0, z)t(z) - (z_0 - z)\overline{G'(z_0, z)t(z)} + \kappa\overline{G(z_0, z)}t(z)] dS(z) \quad (10)$$

where,

$$G(z_0, z) = -\log(z_0 - z) \quad (11)$$

is the Green's function (in complex form) for 2-D potential problems [9, 39], and

$$G'(z_0, z) \equiv \frac{\partial G}{\partial z_0} = -\frac{1}{(z_0 - z)} \quad (12)$$

To discuss the expansions of integrals in Equation (10), we first introduce two auxiliary functions:

$$I_k(z) = \frac{z^k}{k!} \quad \text{for } k \geq 0 \quad (13)$$

$$O_0(z) = -\log(z) \quad \text{and} \quad O_k(z) = \frac{(k-1)!}{z^k} \quad \text{for } k \geq 1 \quad (14)$$

Their derivatives satisfy the following relations:

$$I'_0(z) = 0 \quad \text{and} \quad I'_k(z) = I_{k-1}(z) \quad \text{for } k \geq 1 \quad (15)$$

$$O'_k(z) = -O_{k+1}(z) \quad \text{for } k \geq 0 \quad (16)$$

Also, using the binomial formula, we have

$$I_k(z_1 + z_2) = \sum_{m=0}^k I_{k-m}(z_1)I_m(z_2) \quad \text{for } k \geq 0 \quad (17)$$

We now present the multipole expansions, local expansions and their translations related to Equation (10) in the new fast multipole BEM.

2.1. Multipole expansion (moments)

Assuming z_c is a point close to the integration point z (Figure 2), that is, $|z - z_c| \ll |z_0 - z_c|$, we write:

$$G(z_0, z) = -\log(z_0 - z) = -\log(z_0 - z_c) - \log\left(1 - \frac{z - z_c}{z_0 - z_c}\right)$$

Applying the Taylor series expansion

$$\log(1 - z) = - \sum_{k=1}^{\infty} \frac{z^k}{k} \quad \text{for } |z| < 1$$

and the auxiliary functions introduced in (13) and (14), we obtain

$$G(z_0, z) = \sum_{k=0}^{\infty} O_k(z_0 - z_c) I_k(z - z_c) \quad (18)$$

Note that in this expression for G , z_0 and z are now separated due to the introduction of the ‘mid-point’ z_c , which is a key in the FMM. The first integral in (10) can now be evaluated as follows:

$$\int_{S_0} G(z_0, z) t(z) dS(z) = \int_{S_0} \left[\sum_{k=0}^{\infty} O_k(z_0 - z_c) I_k(z - z_c) \right] t(z) dS(z)$$

that is,

$$\int_{S_0} G(z_0, z) t(z) dS(z) = \sum_{k=0}^{\infty} O_k(z_0 - z_c) M_k(z_c) \quad (19)$$

where

$$M_k(z_c) = \int_{S_0} I_k(z - z_c) t(z) dS(z) \quad \text{for } k \geq 0 \quad (20)$$

are the *first moments* about z_c , which are independent of the collocation point z_0 and only need to be computed once. Similarly, we have

$$\int_{S_0} \overline{G'(z_0, z)} \overline{t(z)} dS(z) = - \sum_{k=0}^{\infty} \overline{O_{k+1}(z_0 - z_c)} \overline{M_k(z_c)} \quad (21)$$

and

$$\int_{S_0} [z \overline{G'(z_0, z)} \overline{t(z)} + \kappa \overline{G(z_0, z)} \overline{t(z)}] dS(z) = \sum_{k=0}^{\infty} \overline{O_k(z_0 - z_c)} N_k(z_c) \quad (22)$$

where the *second moments* are given by

$$N_0 = \kappa \int_{S_0} t(z) dS(z) \quad (23)$$

$$N_k(z_c) = \int_{S_0} [\kappa \overline{I_k(z - z_c)} t(z) - \overline{I_{k-1}(z - z_c)} \overline{z} \overline{t(z)}] dS(z) \quad \text{for } k \geq 1$$

Substituting results in (19), (21) and (22) into Equation (10), we obtain the *multipole expansion*

$$D_t(z_0) = \frac{1}{4\pi\mu(1+\kappa)} \left[\kappa \sum_{k=0}^{\infty} O_k(z_0 - z_c) M_k(z_c) + z_0 \sum_{k=0}^{\infty} \overline{O_{k+1}(z_0 - z_c)} \overline{M_k(z_c)} \right. \\ \left. + \sum_{k=0}^{\infty} \overline{O_k(z_0 - z_c)} N_k(z_c) \right] \quad (24)$$

2.2. Moment-to-moment (*M2M*) translation

If point z_c is moved to a new location $z_{c'}$ (Figure 2), we can write:

$$M_k(z_{c'}) = \int_{S_0} I_k(z - z_{c'}) t(z) dS(z) = \int_{S_0} I_k[(z - z_c) + (z_c - z_{c'})] t(z) dS(z)$$

Applying formula (17), we obtain

$$M_k(z_{c'}) = \sum_{l=0}^k I_{k-l}(z_c - z_{c'}) M_l(z_c) \quad \text{for } k \geq 0 \quad (25)$$

Similarly,

$$N_k(z_{c'}) = \sum_{l=0}^k \overline{I_{k-l}(z_c - z_{c'})} N_l(z_c) \quad \text{for } k \geq 0 \quad (26)$$

These are the *M2M translations* for the moments when z_c is moved to $z_{c'}$. Note that these translation coefficients are symmetrical for the two sets of moments (I_{k-l} and conjugate of I_{k-l}) and coefficients I_{k-l} are exactly the same as in the 2-D potential case [9, 39].

2.3. Local expansion and moment-to-local (*M2L*) translation

Suppose z_L is a point close to the collocation point z_0 (Figure 2), that is, $|z_0 - z_L| \ll |z_c - z_L|$. Expanding $D_t(z_0)$ in (24) about $z_0 = z_L$ and using Taylor series expansion with formula (16), we obtain the following *local expansion*:

$$\begin{aligned} D_t(z_0) &= \sum_{l=0}^{\infty} D_t^{(l)}(z_L) I_l(z_0 - z_L) \\ &= \frac{1}{4\pi\mu(1+\kappa)} \left[\kappa \sum_{l=0}^{\infty} L_l(z_L) I_l(z_0 - z_L) - z_0 \sum_{l=1}^{\infty} \overline{L_l(z_L) I_{l-1}(z_0 - z_L)} \right. \\ &\quad \left. + \sum_{l=0}^{\infty} K_l(z_L) \overline{I_l(z_0 - z_L)} \right] \end{aligned} \quad (27)$$

where the coefficients are given by the following *M2L translations*:

$$L_l(z_L) = (-1)^l \sum_{k=0}^{\infty} O_{l+k}(z_L - z_c) M_k(z_c) \quad \text{for } l \geq 0 \quad (28)$$

$$K_l(z_L) = (-1)^l \sum_{k=0}^{\infty} \overline{O_{l+k}(z_L - z_c)} N_k(z_c) \quad \text{for } l \geq 0 \quad (29)$$

Again, these translations are symmetrical about the two sets of moments and the coefficients are exactly the same as in the 2-D potential case [9, 39].

2.4. Local-to-local translation (*L2L*)

If the point for the local expansion is moved from z_L to $z_{L'}$ (Figure 2), starting with an n -term local expansion in (27) and using formula (17) and the relation $\sum_{l=0}^n \sum_{m=0}^l = \sum_{m=0}^n \sum_{l=m}^n$, we

can show that the new local expansion coefficients are given by the following *L2L translations*:

$$L_l(z_{L'}) = \sum_{m=l}^n I_{m-l}(z_{L'} - z_L) L_m(z_L) \quad \text{for } l \geq 0 \quad (30)$$

$$K_l(z_{L'}) = \sum_{m=l}^n \overline{I_{m-l}(z_{L'} - z_L)} K_m(z_L) \quad \text{for } l \geq 0 \quad (31)$$

where n in the above expressions is the number of terms used in the first local expansion (about the point z_L). Again, these translation coefficients are symmetrical for L_l and K_l , and identical to those used in the 2-D potential case [9, 39].

2.5. Expansions for the T kernel integrals

We now consider the complex representation and multipole expansions for the integrals with the T kernel as given in Equation (5), which can be written as follows using complex variables:

$$\begin{aligned} D_u(z_0) &\equiv [\Delta_1(\mathbf{x}) + i\Delta_2(\mathbf{x})]_u \\ &= -\frac{1}{2\pi(1+\kappa)} \int_{S_0} \{\kappa G'(z_0, z)n(z)u(z) - (z_0 - z)\overline{G''(z_0, z)}n(z)u(z) \\ &\quad + \overline{G'(z_0, z)}[n(z)\overline{u(z)} + \overline{n(z)}u(z)]\} dS(z) \end{aligned} \quad (32)$$

in which $u = u_1 + iu_2$ and $n = n_1 + in_2$. Through a similar procedure as used for the U kernel integrals in (4), the multipole expansion of (32) can be written as

$$\begin{aligned} D_u(z_0) &= \frac{1}{2\pi(1+\kappa)} \left[\kappa \sum_{k=1}^{\infty} O_k(z_0 - z_c) F_k(z_c) + z_0 \sum_{k=1}^{\infty} \overline{O_{k+1}(z_0 - z_c)} F_k(z_c) \right. \\ &\quad \left. + \sum_{k=1}^{\infty} \overline{O_k(z_0 - z_c)} H_k(z_c) \right] \end{aligned} \quad (33)$$

where the moments are:

$$F_k(z_c) = \int_{S_0} I_{k-1}(z - z_c)n(z)u(z) dS(z) \quad \text{for } k \geq 1 \quad (34)$$

$$H_1 = \int_{S_0} [n(z)\overline{u(z)} + \overline{n(z)}u(z)] dS(z) \quad (35)$$

$$\begin{aligned} H_k(z_c) &= \int_{S_0} \{ \overline{I_{k-1}(z - z_c)}[n(z)\overline{u(z)} + \overline{n(z)}u(z)] \\ &\quad - \overline{I_{k-2}(z - z_c)}z_n(z)\overline{u(z)} \} dS(z) \quad \text{for } k \geq 2 \end{aligned}$$

These results are similar to those in Equations (20), (23) and (24) for the U kernel integrals. It can be shown that the M2M, M2L and L2L translations remain the same for the T kernel integrals, except for the fact that $F_0 = H_0 = 0$. That is, the translations used for M_k and N_k can be applied directly to F_k and H_k , respectively. In fact, contributions from F_k will be combined with those from M_k , and contributions from H_k with those from N_k . Therefore, only two sets of moments are involved in the M2M, M2L and L2L translations and each of the three translations uses the same coefficients as in the 2-D potential case [9, 39]. This new fast multipole BEM formulation for 2-D elastostatic problems is therefore very compact and easy to program based on the corresponding fast multipole code for 2-D potential problems [9, 39].

2.6. Fast multipole BEM algorithms

The algorithms in the FMM have been documented in details in many papers (see, e.g. References [9, 24]). For completeness, the main steps are summarized as follows:

Step 1: Discretization. For a given problem, discretize the boundary S as usual as in the conventional BEM (e.g. using constant elements as shown in Figure 3).

Step 2: Determine a quad-tree structure of the elements. Consider a square *cell* that covers the entire boundary S and then start dividing this *parent* cell into four equal *child* cells. Continue dividing in this way until the number of elements in a child cell is less than a pre-specified number (this number is 1 in the example shown in Figure 3). A cell having no child cells is called a *leaf* (shaded cells in Figure 3). A *quad-tree* structure of the cells covering all the elements is thus formed using this procedure (see Reference [24] for more details).

Step 3: Upward pass. Compute the moments on all cells, tracing the tree structure upward (from smaller cells to larger cells). For a leaf, Equations (20) and (23), or (34) and (35)

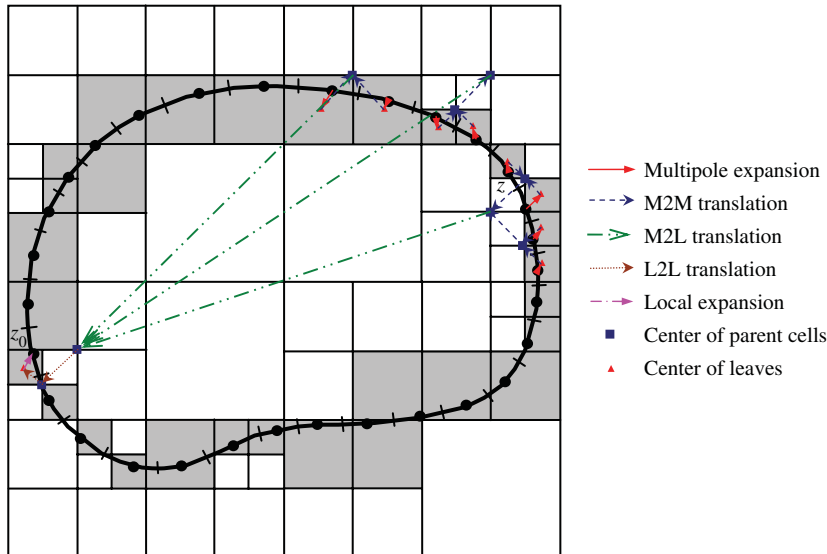


Figure 3. A schematic illustration of the expansions and translations in the fast multipole BEM.

(depending on the boundary conditions) are applied directly (with S_0 being the elements contained in the leaf and z_c the centroid of the leaf). For a parent cell, the moments are calculated by summing the moments on its four child cells using the M2M translation, that is, Equations (25) and (26), in which $z_{c'}$ is the centroid of the parent cell and z_c the centroid of a child cell.

Step 4: Downward pass. Compute the local expansion coefficients on all cells tracing the tree structure downward (from larger cells to smaller cells) until reaching all the leaves. The local expansion coefficients associated with a cell C are the sums of the contributions from the cells in the *interaction list* of cell C (those cells that are not adjacent to C but their parent cells are adjacent to C 's parent cell [24]) and from all the far cells. The former are calculated by using the M2L translation, Equations (28) and (29), and the latter are calculated by using the L2L translation, Equations (30) and (31).

Step 5: Evaluation of integrals in (4) or (5). Compute the contributions from elements in leaf C and its adjacent cells directly as in the conventional BEM. Contributions from all other cells (cells in the interaction list of C and far cells) are computed by using the local expansion, e.g. Equation (27). This is done by using the local expansion coefficients for cell C , computed in Step 4, and shifting the expansion point from the centroid of C to the collocation point z_0 (Figure 3; see Reference [24] for more details).

Step 6: Iterations of the solution. Update the unknown vector in the system $\mathbf{A}\lambda = \mathbf{b}$ corresponding to BIE (1), and continue at Step 3 for the multiplication of matrix and unknown vector until the solution converges within a given tolerance.

Pre-conditioners for the fast multipole BEM are crucial for its convergence and computing efficiency. In this study, the block diagonal pre-conditioner is employed, which is formed on each leaf using direct evaluations of the kernels on the elements within that leaf. When the problem size is large, the estimated cost of the entire process described above is $O(N)$ with N being the number of equations, if the number of terms in the multipole expansions and the number of elements in a leaf are kept constant (see Reference [24] for the estimates).

In this study, we employ the constant boundary elements (straight-line segment with one node) to discretize the BIE. Although constant elements are less accurate compared with other higher-order elements, there are some compelling reasons to employ them with the fast multipole BEM. First, with constant elements, all integrals can be evaluated analytically and there is no need to use any numerical integrations. Second, because of the analytical integrations, the difficulties with nearly singular integrals are not present no matter how close two parts of the boundary can become. In the developed program, all the moments given in Equations (20), (23), (34) and (35) are evaluated analytically, as well as the direct integrations of the U and T kernels in the near-field evaluations. In this way, the program can be very efficient and robust.

3. NUMERICAL EXAMPLES

We present three numerical examples to demonstrate the accuracy and efficiency of the new fast multipole BEM for 2-D elasticity problems. All the computations were done on a Pentium IV laptop with a 2.4GHz CPU and 1GB RAM. In all cases, the material has a Young's modulus E and Poisson's ratio ν .

3.1. A cylinder with pressure loads

We first consider a thick cylinder under pressure loads (in the plane strain case) as shown in Figure 4. The inner pressure is p_i and the outer pressure is p_o . In the case studied, $b=2a$, $p_i=p_o=p$, and Poisson's ratio $\nu=0.3$. We discretize the inner and outer boundaries with the same number of elements and run both the fast multipole BEM code and a conventional BEM code, which also uses constant elements and analytical integrations. The conventional BEM code uses both the direct solver (LAPACK) and the iterative solver (GMRES) for solving the linear system. For the fast multipole BEM, the numbers of terms for both multipole and local expansions were set to 20, the maximum number of elements in a leaf to 20, and the tolerance for convergence of the solution to 10^{-6} . All the fast multipole BEM results converged in about 3 iterations without using any pre-conditioner in this example.

Table I shows the results of radial displacement component u_r and hoop stress σ_θ at the inner boundary using both the fast multipole BEM and the conventional BEM (with the direct

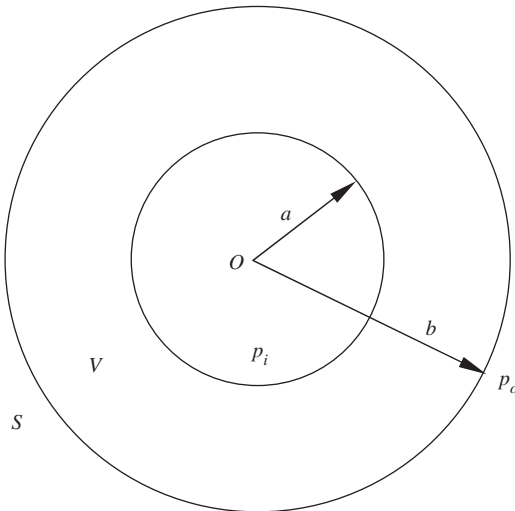


Figure 4. A thick cylinder with pressure loads.

Table I. Radial displacement and hoop stress at the inner boundary.

DOFs	$u_r(\times pa/E)$		$\sigma_\theta(\times p)$	
	Conventional BEM	Fast multipole BEM	Conventional BEM	Fast multipole BEM
400	-0.52233	-0.52233	-1.00228	-1.00228
720	-0.52143	-0.52143	-1.00149	-1.00148
1440	-0.52076	-0.52076	-1.00081	-1.00082
2880	-0.52039	-0.52039	-1.00042	-1.00042
4800	-0.52024	-0.52024	-1.00026	-1.00026
9600	-0.52012	-0.52012	-1.00013	-1.00007
Exact solution	-0.52000		-1.00000	

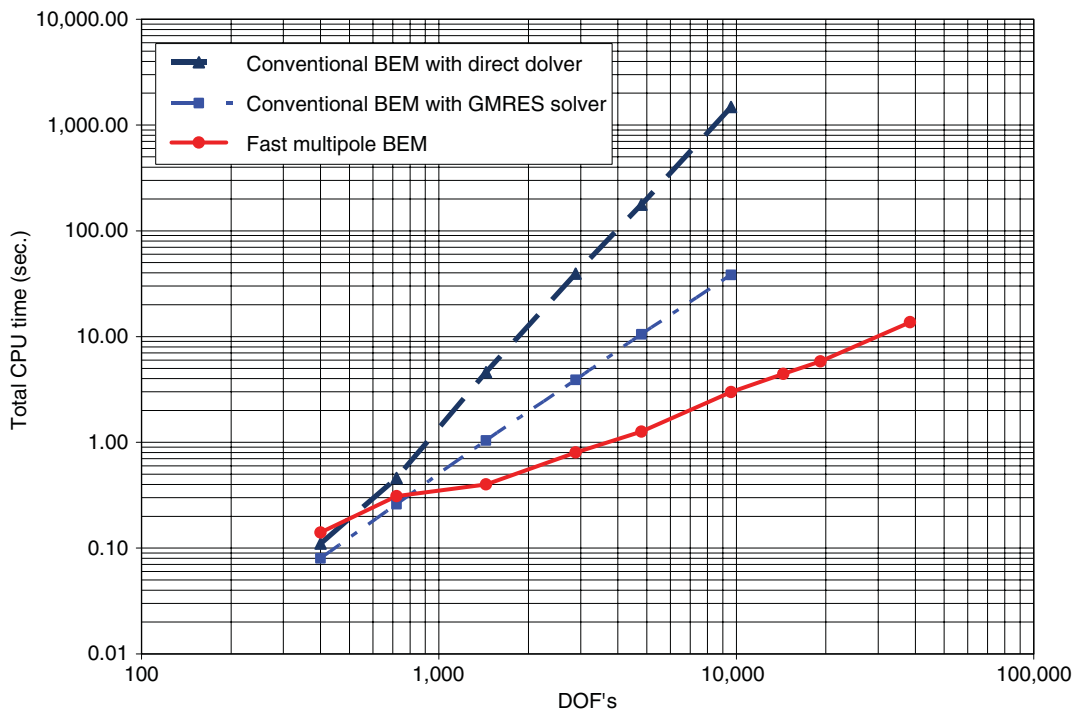


Figure 5. Comparison of the CPU time used by the conventional BEM and fast multipole BEM.

solver) as the total number of elements increases from 200 to 4800 (degrees of freedom from 400 to 9600). As we can see, the results for both fast multipole BEM and conventional BEM converge quickly to the exact solution [40] for the mesh with 360 constant elements with a relative error of less than 3%. The results continue to improve with the increase in the number of elements.

The CPU times used for the two BEM approaches are plotted in Figure 5, which shows significant advantage of the fast multipole BEM compared with the conventional BEM with either direct or iterative solver. For example, for the model with 4800 elements (DOFs = 9600), the fast multipole BEM used 3 s of the CPU time, while the conventional BEM used 1483 s with the direct solver and 38 s with the iterative solver. Beyond 10 000 DOFs, the conventional BEM (with double precision) encounters the 1 GB physical memory barrier and cannot run efficiently using the virtual memory. It is also interesting to note from Figure 5 that the slopes of the three curves for the conventional BEM with direct solver, iterative solver, and the fast multipole BEM are close to 3, 2, and 1 on the log–log scales, suggesting the $O(N^3)$, $O(N^2)$ and $O(N)$ efficiencies of the three methods, respectively.

This example shows that the fast multipole BEM is very efficient compared with the conventional BEM. In addition, the fast multipole BEM results are equally accurate as the conventional BEM results, and they are very stable with the increase in the model size.

3.2. A square plate with a circular hole

In the second example, we further study the accuracy of the fast multipole BEM using a stress concentration problem—a square plate with a circular hole at the centre, as shown in Figure 6. The edge length of the square plate is a and radius of the hole is $R = 0.1a$. The plate is loaded in the x -direction with a uniform load p , and Poisson's ratio $\nu = 0.3$ in this study. The maximum (at point A) and minimum (at point B) hoop stresses on the edge of the hole are sought (Figure 6) using both the fast multipole BEM code and ANSYS, a finite element method (FEM) package. In the BEM models, numbers of boundary elements on the edge of the hole increase while that on the outer edges of the plate is kept at 100, except for the last BEM model in which 200 elements are used on the outer edges of the plate. The numbers of terms for both multipole and local expansions were set to 20, the maximum number of elements in a leaf to 100, and the tolerance for convergence to 10^{-6} . All the fast multipole BEM results converged in about 20 iterations. In the FEM models, 4-node quadrilateral elements are used in order to compare with the BEM models (which use constant boundary elements). In the FEM meshes, smaller elements are used near the hole while larger elements are used near the outer boundaries of the plate.

Table II shows the comparison of the computed hoop stresses at points A and B . For an infinitely large plate with a hole, the hoop stress at point A is $3p$, while that at point B is

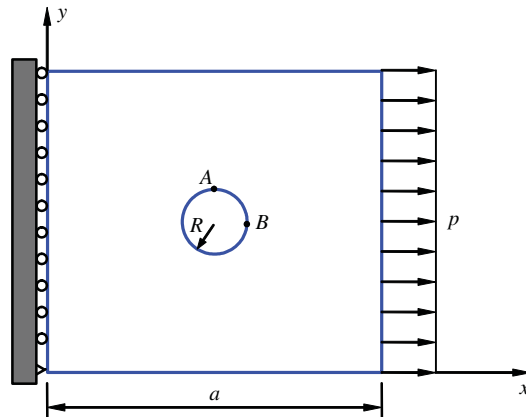


Figure 6. A square plate with a circular hole at the centre and loaded with p .

Table II. Computed hoop stress $\sigma_\theta (\times p)$ on the edge of the hole.

Fast multipole BEM			FEM		
DOFs	At point A	At point B	DOFs	At point A	At point B
560	3.215	-1.176	1206	3.148	-1.101
920	3.216	-1.183	4522	3.229	-1.185
1640	3.216	-1.185	9490	3.225	-1.187
3080	3.217	-1.188	38440	3.226	-1.192
7600	3.222	-1.190			

$-p$ [40]. For our finite sized plate with the hole, the hoop stresses should be slightly higher than these values. The stress values for both fast multipole BEM (with DOFs = 1640) and FEM (with DOFs = 4522) converged quickly to around $3.22p$ at point A and $-1.19p$ at point B. Further increases in the numbers of elements provided little improvements in the results. This example demonstrates again that the results using fast multipole BEM code are accurate and stable.

It should be pointed out that the element types used for both the BEM and FEM in this study are the simplest elements available. If higher-order elements such as quadratic elements are used, a few hundred elements should be sufficient for both the BEM and FEM to achieve the same accuracy as reported in this example.

3.3. Square perforated plates

Next, we study perforated plates, or plates with many circular holes, distributed uniformly or randomly (Figure 7). The effective elastic moduli of the plates are evaluated by using the developed fast multipole BEM. Several models of the plates, with increasing dimensions and thus the number of holes, are considered. Each model of the plate has a dimension of $m \times m$, containing a total of $2m \times 2m$ holes, with $m = 1, 2, 3, 4, 6, 10, 15$, and 20. The radii of the holes are the same (0.1) for all the models that gives a total ‘volume’ fraction of the holes equal to 12.57%. Each hole is discretized with 360 elements and the outer four straight edges of the plate are discretized with $400m$ elements. Thus, the largest model (shown in Figure 7) with 1600 holes ($m = 20$) has a total DOFs of 1 168 000. The same boundary conditions and material property, as used in the previous example (Figure 6), are applied in this case (traction-free boundary conditions are applied on all edges of the holes). Using this model, the effective Young’s modulus E_{eff} of the perforated plate can be estimated by the following simple formula:

$$E_{\text{eff}} = \frac{pa}{u_{\text{ave}}}$$

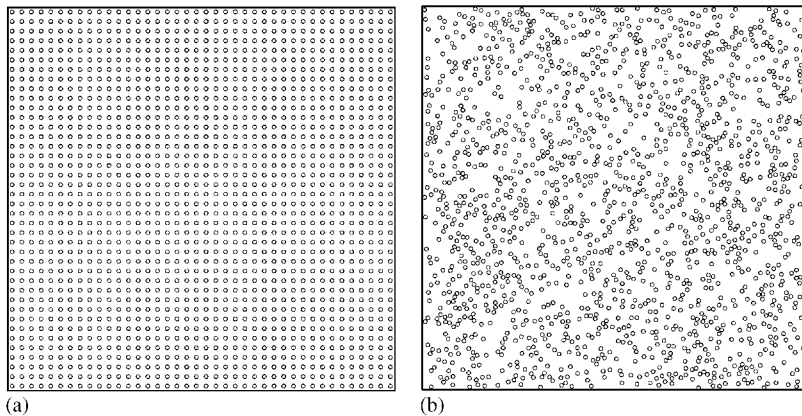


Figure 7. BEM models of perforated plates (with 1600 circular holes): (a) uniform distribution; and (b) random distribution.

Table III. Computed effective Young's moduli for the perforated plates.

Models		Uniformly distributed holes	Randomly distributed holes		
No. holes	DOFs	$E_{\text{eff}}(\times E)$	No. iterations	$E_{\text{eff}}(\times E)$	No. iterations
2 × 2	3680	0.697892	25	0.678698	26
4 × 4	13 120	0.711998	31	0.682582	31
6 × 6	28 320	0.715846	29	0.659881	40
8 × 8	49 280	0.717643	28	0.651026	40
12 × 12	108 480	0.719345	28	0.672084	39
20 × 20	296 000	0.720634	29	0.676350	35
30 × 30	660 000	0.721255	30	0.676757	36
40 × 40	1 168 000	0.721558	35	0.675261	38

where u_{ave} is the averaged displacement u_1 (at $x=a$) and p the applied load (Figure 6). In this example, the numbers of terms for both expansions were set to 20, the maximum number of elements in a leaf to 100, and the tolerance for convergence to 10^{-6} .

Table III shows the calculated effective Young's moduli using the fast multipole BEM for plates with both uniformly and randomly distributed holes. For the plate with uniformly distributed holes, theoretically speaking, the calculated E_{eff} should be independent of the sizes of the models used. The results however show slight derivations among the models, as shown in Table III. This is because that we did not apply the periodic boundary condition or impose the simplified 'straight-line' boundary condition for the upper and lower edges of the plate [41], to account for the interactions from the surrounding materials. This 'boundary' effect diminishes when the size of the model increases. For the case with randomly distributed holes, the estimated E_{eff} oscillates initially and then approaches a fixed value as the model size increases, as expected. The estimated Young's modulus for the random distribution case ($E_{\text{eff}}=0.675E$) is slightly lower than that in the uniform distribution case ($E_{\text{eff}}=0.722E$), which suggests that the random distribution may reduce the load transfer capability of the perforated plate. These values of the computed E_{eff} are very close to those reported in Reference [42]. The numbers of iterations for each case are also listed in Table III.

The CPU time used for the models with both uniformly and randomly distributed holes are shown in Figure 8. It is seen that both curves have a slope close to unity on the log-log scales, which clearly demonstrates the $O(N)$ efficiency of the developed fast multipole BEM in solving large-scale 2-D elasticity problems. The largest model with more than one million DOFs is solved in 4 h as shown in Figure 8. In comparison, in Reference [21], where a 2-D fast multipole BEM based on direct expansions of the kernels in real variables is presented, more than 31 h are used on a similar Pentium IV desktop computer for a 2-D BEM model of an inclusion problem with 544 000 DOFs and also using constant elements.

4. DISCUSSIONS

A new fast multipole BEM formulation for solving large-scale 2-D elastostatic problems is presented in this paper based on the direct BIE and representations of the kernels with complex analytic functions. The new formulation is shown to be linked directly to the fast multipole BEM for 2-D potential problems. As in the 2-D potential case, complex potentials in the 2-D

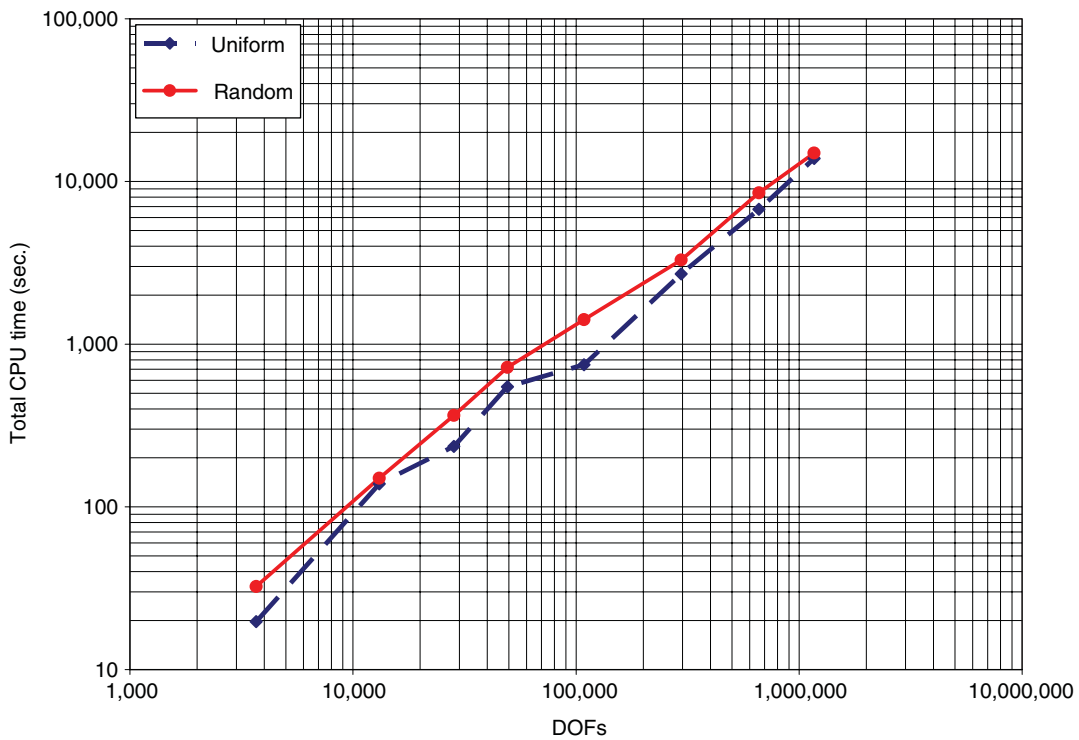


Figure 8. Total CPU time used by the fast multipole BEM for solving the perforated plate problems (log–log scale).

elasticity are employed to represent the integrations of the kernels in the far field, yielding a very compact formulation. The resulting M2M, M2L and L2L translations are identical to those for the 2-D potential problems and are symmetrical about the two sets of moments. Thus, programming is straightforward for the new 2-D elasticity fast multipole BEM based on any fast multipole BEM code for 2-D potential problems. Three numerical examples are presented that clearly demonstrate the accuracy and efficiency of the developed fast multipole BEM for solving large-scale 2-D elasticity problems.

To improve the accuracy of the fast multipole BEM code, constant elements can certainly be replaced by higher-order elements. For constant elements, all the integrals are evaluated analytically, for all non-singular, nearly singular and singular cases. There are no numerical integrations at all in the code. The code is thus very efficient and accurate even when boundaries are closely packed together as in the third example in the previous section. For higher-order elements, however, this may no longer be the case (unless the elements are straight or circular-arc segments [43]). In general, one will need to use numerical integrations or other schemes for the direct evaluations of singular and nearly singular integrals. This may reduce the efficiency in the fast multipole BEM solutions. Nevertheless, higher-order elements may still be needed in critical applications such as fracture analysis.

From this and many other studies, it is clear that the fast multipole BEM is suitable for analysing many large-scale problems, such as modelling of composites, porous materials and

MEMS. Fast multipole BEM for dynamic, non-linear and coupled-field problems will be interesting and challenging topics in these applications.

ACKNOWLEDGEMENTS

The author would like to thank Professor Naoshi Nishimura at Kyoto University and Professor Takuo Fukui at Fukui University for numerous discussions and their help in the research on the fast multipole BEM in general. The author also thanks the three reviewers for their useful suggestions in improving this manuscript.

REFERENCES

1. Rizzo FJ. An integral equation approach to boundary value problems of classical elastostatics. *Quarterly of Applied Mathematics* 1967; **25**:83–95.
2. Mukherjee S. *Boundary Element Methods in Creep and Fracture*. Applied Science Publishers: New York, 1982.
3. Cruse TA. *Boundary Element Analysis in Computational Fracture Mechanics*. Kluwer Academic Publishers: Dordrecht, The Netherlands, 1988.
4. Brebbia CA, Dominguez J. *Boundary Elements—An Introductory Course*. McGraw-Hill: New York, 1989.
5. Banerjee PK. *The Boundary Element Methods in Engineering* (2nd edn). McGraw-Hill: New York, 1994.
6. Kane JH. *Boundary Element Analysis in Engineering Continuum Mechanics*. Prentice Hall: Englewood Cliffs, NJ, 1994.
7. Rokhlin V. Rapid solution of integral equations of classical potential theory. *Journal of Computational Physics* 1985; **60**:187–207.
8. Greengard LF, Rokhlin V. A fast algorithm for particle simulations. *Journal of Computational Physics* 1987; **73**(2):325–348.
9. Greengard LF. *The Rapid Evaluation of Potential Fields in Particle Systems*. The MIT Press: Cambridge, MA, 1988.
10. Peirce AP, Napier JAL. A spectral multipole method for efficient solution of large-scale boundary element models in elastostatics. *International Journal for Numerical Methods in Engineering* 1995; **38**:4009–4034.
11. Greengard LF, Kropinski MC, Mayo A. Integral equation methods for Stokes flow and isotropic elasticity in the plane. *Journal of Computational Physics* 1996; **125**:403–414.
12. Greengard LF, Helsing J. On the numerical evaluation of elastostatic fields in locally isotropic two-dimensional composites. *Journal of the Mechanics and Physics of Solids* 1998; **46**(8):1441–1462.
13. Fu Y, Klimkowski KJ, Rodin GJ, Berger E, Browne JC, Singer JK, Geijn RAVD, Vemaganti KS. A fast solution method for three-dimensional many-particle problems of linear elasticity. *International Journal for Numerical Methods in Engineering* 1998; **42**:1215–1229.
14. Yoshida K, Nishimura N, Kobayashi S. Application of fast multipole Galerkin boundary integral equation method to crack problems in 3D. *International Journal for Numerical Methods in Engineering* 2001; **50**:525–547.
15. Yoshida K, Nishimura N, Kobayashi S. Application of new fast multipole boundary integral equation method to elastostatic crack problems in three dimensions. *Journal of Structural Engineering (JSCE)* 2001; **47A**: 169–179.
16. Richardson JD, Gray LJ, Kaplan T, Napier JA. Regularized spectral multipole BEM for plane elasticity. *Engineering Analysis with Boundary Elements* 2001; **25**:297–311.
17. Popov V, Power H. An O(N) Taylor series multipole boundary element method for three-dimensional elasticity problems. *Engineering Analysis with Boundary Elements* 2001; **25**(1):7–18.
18. Popov V, Power H, Walker SP. Numerical comparison between two possible multipole alternatives for the BEM solution of 3D elasticity problems based upon Taylor series expansions. *Engineering Analysis with Boundary Elements* 2003; **27**(5):521–531.
19. Lai Y-S, Rodin GJ. Fast boundary element method for three-dimensional solids containing many cracks. *Engineering Analysis with Boundary Elements* 2003; **27**(8):845–852.
20. Masters N, Ye W. Fast BEM solution for coupled 3D electrostatic and linear elastic problems. *Engineering Analysis with Boundary Elements* 2004; **28**(9):1175–1186.

21. Yao Z, Kong F, Wang H, Wang P. 2D simulation of composite materials using BEM. *Engineering Analysis with Boundary Elements* 2004; **28**(8):927–935.
22. Liu YJ, Nishimura N, Otani Y, Takahashi T, Chen XL, Munakata H. A fast boundary element method for the analysis of fiber-reinforced composites based on a rigid-inclusion model. *Journal of Applied Mechanics* 2005; **72**(1):115–128.
23. Liu YJ, Nishimura N, Otani Y. Large-scale modeling of carbon-nanotube composites by the boundary element method based on a rigid-inclusion model. *Computational Materials Science* 2005; **34**(2):173–187.
24. Nishimura N. Fast multipole accelerated boundary integral equation methods. *Applied Mechanics Reviews* 2002; **55**(4):299–324.
25. Nishimura N, Yoshida K, Kobayashi S. A fast multipole boundary integral equation method for crack problems in 3D. *Engineering Analysis with Boundary Elements* 1999; **23**:97–105.
26. Yoshida K, Nishimura N, Kobayashi S. Application of new fast multipole boundary integral equation method to crack problems in 3D. *Engineering Analysis with Boundary Elements* 2001; **25**:239–247.
27. Yamada Y, Hayami K. *A Multipole Boundary Element Method for Two Dimensional Elastostatics*, Department of Mathematical Engineering and Information Physics, University of Tokyo, 1995; 1–20.
28. Muskhelishvili NI. *Some Basic Problems of Mathematical Theory of Elasticity*. Noordhoff: Groningen, 1958.
29. Sokolnikoff IS. *Mathematical Theory of Elasticity*. McGraw Hill: New York, 1956.
30. Lee KJ. A boundary element method for plane isotropic elastic media using complex variable technique. *Computational Mechanics* 1993; **11**:83–91.
31. Denda M, Dong YF. Complex variable approach to the BEM for multiple crack problems. *Computer Methods in Applied Mechanics and Engineering* 1997; **141**(3–4):247–264.
32. Fukui T. Research on the boundary element method—development and applications of fast and accurate computations. *Ph.D. Dissertation*, Kyoto University, 1998.
33. Mogilevskaya SG, Linkov AM. Complex fundamental solutions and complex variables boundary element method in elasticity. *Computational Mechanics* 1998; **22**(1):88–92.
34. Linkov AM, Mogilevskaya SG. Complex hypersingular BEM in plane elasticity problems. In *Singular Integrals in Boundary Element Method*, Sladek V, Sladek J (eds). Computational Mechanics Publications: Southampton, 1998; 299–364.
35. Chau KT, Wang YB. A new boundary integral formulation for plane elastic bodies containing cracks and holes. *International Journal of Solids and Structures* 1999; **36**(14):2041–2074.
36. Gadala MS, Tang SG. Complex variable BEM solution for half-plane problems with straight boundary clamped. *International Journal of Solids and Structures* 1999; **36**(26):4017–4029.
37. Linkov AM. *Boundary Integral Equations in Elasticity Theory*. Kluwer Academic Publishers: Dordrecht, 2002.
38. Koshelev V, Ghassemi A. Complex variable BEM for thermo- and poroelasticity. *Engineering Analysis with Boundary Elements* 2004; **28**(7):825–832.
39. Liu YJ, Nishimura N. The fast multipole boundary element method for potential problems—a tutorial, 2005, in review.
40. Timoshenko SP, Goodier JN. *Theory of Elasticity* (3rd edn). McGraw-Hill: New York, 1987.
41. Liu YJ, Xu N, Luo JF. Modeling of interphases in fiber-reinforced composites under transverse loading using the boundary element method. *Journal of Applied Mechanics* 2000; **67**(1):41–49.
42. Hu N, Wang B, Tan GW, Yao ZH, Yuan WF. Effective elastic properties of 2-D solids with circular holes: numerical simulations. *Composites Science and Technology* 2000; **60**(9):1811–1823.
43. Mogilevskaya SG. The universal algorithm based on complex hypersingular integral equation to solve plane elasticity problems. *Computational Mechanics* 1996; **18**(2):127.